Available online at www.sciencedirect.com

ScienceDirect

journal homepage: www.elsevier.com/locate/he

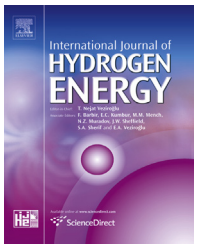

Mg-based nanocomposites with improved hydrogen storage performances

Tong Liu [a,*], *Chenxi Wang* [a], *Ying Wu* [b,c,**]

[a] *Key Laboratory of Aerospace Materials and Performance (Ministry of Education), School of Materials Science and Engineering, Beihang University, Beijing 100191, China*

[b] *School of Materials Science and Engineering, Shanghai Institute of Technology, No. 120, Cao Bao Road, Shanghai 200235, China*

[c] *China Iron & Steel Research Institute Group, Advanced Technology & Materials Co., Ltd, No. 76 Xueyuannanlu, Haidian District, Beijing 100081, China*

ARTICLE INFO

Article history:
Received 25 October 2013
Received in revised form
17 March 2014
Accepted 18 March 2014
Available online 16 April 2014

Keywords:
Magnesium
Nanocomposite
Hydrogen plasma-metal reaction
Rapid solidification
Hydrogen storage

ABSTRACT

MgH_2 is one of the most attractive candidates for on-board H_2 storage. However, the practical application of MgH_2 has not been achieved due to its slow hydrogenation/dehydrogenation kinetics and high thermodynamic stability. Many strategies have been adopted to improve the hydrogen storage properties of Mg-based materials, including modifying microstructure by ball milling, alloying with other elements, doping with catalysts, and nanosizing. To further improve the hydrogen storage properties, the nanostructured Mg is combined with other materials to form nanocomposite. Herein, we review the recent development of the Mg-based nanocomposites produced by hydrogen plasma-metal reaction (HPMR), rapid solidification (RS) technique, and other approaches. These nanocomposites effectively enhance the sorption kinetics of Mg by facilitating hydrogen dissociation and diffusion, and prevent particle sintering and grain growth of Mg during hydrogenation/dehydrogenation process.

Introduction

Hydrogen, the lightest element, burns with oxygen and emits only environmentally friendly water. The hydrogen energy system was first proposed to solve the worldwide oil crisis in 1970s. In recent years, hydrogen has drawn growing attentions from scientists and automotive industries as the ideal candidate for energy carrier to replace the fossil fuel-based economy. However, the widespread use of hydrogen is still challenged by its storage technology, especially for the applications in the vehicles powered by fuel cells and in the hydrogen fueled internal combustion engines. To realize the hydrogen economy, the development of a safe and efficient hydrogen storage approach is the key issue. The US Department of Energy (DOE) published a long-term goal for hydrogen-storage applications, and the required minimum hydrogen-storage capacity should be 6.5 wt.% and 65 g L^{-1} hydrogen at the temperature between 333 and 393 K [1]. The conventional hydrogen storage approaches through the compressed

* *Corresponding author*. Key Laboratory of Aerospace Materials and Performance (Ministry of Education), School of Materials Science and Engineering, Beihang University, Beijing 100191, China.

** *Corresponding author*. School of Materials Science and Engineering, Shanghai Institute of Technology, No. 120, Cao Bao Road, Shanghai 200235, China.

E-mail addresses: tongliu@buaa.edu.cn (T. Liu), yingwu2000@hotmail.com (Y. Wu).

http://dx.doi.org/10.1016/j.ijhydene.2014.03.125

hydrogen gas and the cryogenic hydrogen liquid are not capable of meeting the targets of DOE for the on-board applications, e.g. high hydrogen storage capacity, safety and low cost. Hydrogen storages via metal hydride materials have the potential advantages of high volumetric and gravimetric capacities and safety [2]. So far, many kinds of hydrogen storage materials have been developed, e.g. $LaNi_5$ [3], Mg_2Ni [4], alanates [5], amides [6] and borohydrides [7]. Nevertheless, these materials fail to satisfy all the necessary requirements due to the drawbacks, including unfavorable thermodynamics, poor kinetics, irreversibility, and releasing undesirable by-products.

Features of magnesium hydrides

Among the metal hydrides, MgH_2 is still one of the most attractive candidates for hydrogen storage due to its high theoretical gravimetric capacity of 7.6 wt.%, volumetric capacity of 110 $g\,L^{-1}$, energy density of 9 $MJ\,kg^{-1}$, abundance, reversibility and low cost [2]. Moreover, MgH_2 possesses other advantages, such as heat-resistance, vibration absorbing and recyclability. In recent years, much attention has been paid to develop novel Mg-based hydrogen storage materials. Up to now, the practical application of MgH_2, however, has not been achieved due to its slow hydrogenation/dehydrogenation kinetics and high thermodynamic stability. MgH_2 must be heated to 623–673 K under a hydrogen pressure of more than 3 MPa to achieve an adequate rate of hydrogenation/dehydrogenation [8].

There are three main factors that significantly hinder the hydrogen absorption/desorption rate of Magnesium. Firstly, a highly stable MgO layer is often formed on the surface of the Mg particles and prevents the diffusion of hydrogen into Mg. In order to break down the oxide layer, the activation process is often carried out through annealing Mg at 673 K in vacuum and in hydrogen for several cycles. Andreasen et al. found that with the presence of MgO surface layer, the Mg-based materials showed large apparent activation energies due to the delayed hydrogen diffusion, whereas the well activated samples exhibited smaller activation energies [9]. Nevertheless, even after the activation process, Mg in microscale can absorb only 1.5 wt.% H_2 within 2 h at 673 K [10]. The second reason for the slow rate of hydrogenation is the low dissociation rate of hydrogen molecules on the surface of Mg [11]. Without catalytic additives, the dissociation of hydrogen molecules on the surface of magnesium requires high activation energy. Thirdly, after the formation of MgH_2 on the surface of Mg, the diffusion of hydrogen through this hydride layer becomes the dominant factor for the hydrogenation process because the diffusion rate of hydrogen in MgH_2 is lower than in Mg [12,13]. It was also reported that the hydrogenation rate of Mg decreased with the increasing hydride layer thickness [14]. When the thickness of hydride layer exceeded a critical value of 30–50 μm, the hydrogenation reaction even stopped [10,15].

Approaches to improve the hydrogen storage properties of magnesium hydride

In the past two decades, many efforts have been devoted to reduce the operation temperature and improve the hydrogenation/dehydrogenation kinetics of the Mg-based materials via modifying microstructure by ball milling, alloying with other elements, doping with catalysts, and nanosizing.

Ball milling not only creates fresh surfaces, but also can induce structural defects, phase change, and nanostructure [16,17]. By the mechanical milling or alloying method, the crystalline size of the Mg-based materials can be reduced to nanometer scale, which offers more diffusion channels for hydrogen. Moreover, the induced microstrain also assists diffusion by reducing the hysteresis of hydrogen absorption and desorption [18]. However, the grain boundary effect due to the nanocrystalline does not dramatically change the pressure-composition (P–C) isotherms. Milling under hydrogen atmosphere has also been adopted to prepare the Mg-based hydrides [19]. In this approach, ball milling causes hydrogen uptake and mechanical deformation simultaneously. Therefore, the nanostructured Mg-based materials often exhibit much higher hydrogen storage capacity and fast sorption kinetics as well [10].

Chemical composition is one of the most important factors to determine the hydrogen storage properties [20]. The Mg-based materials alloyed with other elements have shown rapid hydrogenation/dehydrogenation kinetics and a reduced operation temperature [21–25]. Mechanical alloying is often adopted to synthesize the Mg-based hydrogen storage alloys, such as Mg–Ni [21,22] and Mg–Co [23,24]. Mg_2Ni can react with hydrogen to form Mg_2NiH_4 at 470–500 K [25]. The standard enthalpy of this reaction was found to be 65 kJ mol^{-1} H_2, lower than that of MgH_2 (78 kJ mol^{-1} H_2) [26]. Akiba group produced the Mg–Co alloys by mechanical alloying method [24,27]. They found that the $Mg_{50}Co_{50}$ alloy with both crystalline BCC phase and amorphous-like phase had a particle size of 1–2 μm and a grain size of about a few nanometers [28]. It can absorb 2 wt.% hydrogen at 303 K in 1 h under an initial hydrogen pressure of 3.3 MPa. By using Mg, Ni, Co, Cu and Fe nanoparticles, Shao and Liu et al. [29,30] also synthesized the nanostructured Mg-based compounds (Mg_2Ni, Mg_2Co, Mg_2Cu and Mg_2FeH_6) with high purity by gas–solid reaction in much mild. For example, the Mg_2Ni nanoparticles of 50 nm can be prepared at 523 K under 4 MPa H_2. The nanostructure of these samples greatly enhanced the kinetic properties of hydrogen absorption and desorption. The Mg_2Ni nanoparticles can absorb 3.4 wt.% hydrogen in several minutes at 493 K. Furthermore, the sorption kinetics of the nanostructured Mg_2Ni was almost stable during ten cycles [30]. The thermodynamic properties of these nanostructured Mg_2M were improved slightly as well.

Catalyst is another critical factor to promote the hydrogen sorption kinetics in Mg. The transition metals (Fe, Ni, Ti, V, Cu, Co) [31–33], oxides [34], halides [35], and intermetallic compounds [36–38] can catalyze the dissociation of H_2 molecules on the surface of Mg. The mobile H atoms induce fast diffusion rate into Mg crystal lattice, enhance the kinetics of hydrogenation/dehydrogenation, and increase the hydrogen storage capacity at the moderate temperatures [32]. Fujii et al. [39] found that MgH_2 sample doped with 1 mol% Nb_2O_5 absorbed 4.5 wt.% hydrogen at room temperature under a hydrogen pressure of 1 MPa.

Recent theoretical simulations have suggested that when the particle size of Mg is reduced to nanoscale, both the

hydrogen absorption and desorption kinetics can be significantly improved [16,40,41]. Metal hydride particles with grain size of 10–50 nm are usually prepared by high-energy ball milling. However, this technique can hardly decrease the particle size to nanoscale and is inadequate to produce a dramatic size effect. Mg nanoparticles have been prepared by several routes, including organometallic chemistry [42,43], solution-processing using colloidal chemistry [44,45], sonoelectrochemistry [46], and gas-phase methods [47,48]. The nanoscale Mg exhibited far superior hydrogen storage properties to the Mg in microscale [49].

Mg-based nanocomposites with improved hydrogen storage properties

To further improve the hydrogen storage properties, recently, the Mg nanoparticle or nanocrystalline has been combined with other materials to form nanocomposite. High energy ball-milling (HEBM) approach is often adopted to produce the Mg-based nanocomposites [50,51]. The Mg–TiH_2 nanocomposite exhibited rapid absorption kinetics, and the activation energy of desorption for magnesium hydride was reduced to 473 K. On the other hand, Mg nanoparticles are very reactive towards oxygen [52]. The oxide layer of these nanoparticles impeded the hydrogen diffusion and decreased the hydrogen storage performance. To improve both the durability and the hydrogen sorption kinetics of Mg, the Mg-based nanocomposites have been developed through surface modification or nanoconfinement [53,54]. Nanocomposites enhance the sorption kinetics of Mg due to the shorter diffusion length for hydrogen and the higher nucleation rate, prevent particle sintering and grain growth of Mg during hydrogenation/dehydrogenation process, and possibly destabilize the hydride phase. Hereafter, we review the recent achievements in the Mg-based nanocomposites produced by HPMR, RS technique, and other approaches.

Mg-based nanocomposites synthesized by HPMR approach

Krishnan and co-workers [55,56] endeavored to cover Mg nanoparticles with metallic layer by inert gas condensation technique. They produced the Mg–Ti nanoparticles by magnetron sputtering a target of Mg and Ti mixture in an inert Kr atmosphere [55]. The addition of Ti reduced the size of Mg nanoparticles to 5–20 nm. However, the Mg nanoparticles were covered with magnesium oxide shell of 3–4 nm in thickness, and the Ti nanoparticles were separated from the Mg nanoparticles. The Mg–Ni binary system has also been tested by the same group [56]. They only observed the Mg_2Ni nanoparticles covered with Ni, nevertheless, the Mg nanoparticles covered with metallic shell have not been successfully prepared yet. Thus, it is still very challenging to cover the Mg nanoparticles with a metallic shell by using the conventional technique.

HPMR method is a novel vapor deposition processing and suitable for producing metallic nanoparticles industrially with high purity and low cost. In this approach, bulk metals are vaporized by arc plasma in a mixture of Ar and H_2 atmosphere. The metal vapors are taken to a collecting filter by circulation gas. Before being taken out from the collecting room, the metal nanoparticles are passivated by a mixture of Ar and air to prevent them from burning. Up to now, nanoparticles of various alloys and intermetallics have been fabricated by using HPMR approach, and the particle size can be tuned by controlling the hydrogen pressure and the current value [57–59]. Recently, we have designed and fabricated several types of Mg-based nanocomposites, such as Mg–Zn, Mg–V, Mg–Al, Mg–La–Al and Mg–La–Ni nanocomposites, by HPMR approach to create a metallic coating on the Mg nanoparticles [60–64].

Mg–V nanocomposite

It is known that vanadium can absorb and release hydrogen under moderate pressure and temperature [65,66]. Liang et al. [66] found that the ball-milled MgH_2–5 at.% V nanocrystalline desorbed hydrogen completely within 1000 s at 523 K. Kondo and Sakurai [67] demonstrated that Mg_2CaV_3 ternary alloy prepared by mechanical alloying could absorb 3.3 wt.% even at 298 K. According to the Mg–V binary diagram, they are immiscible in solid state [68], and therefore it is possible to create the Mg-based nanocomposite with V hydride dispersed on the surface of Mg during the HPMR processing.

Liu et al. [60] prepared the Mg–10.2 at.% V composite nanoparticles from the Mg and V ingots by HPMR method. These nanoparticles are made of Mg, VH_2 and a small amount of MgH_2. The Mg nanoparticles are hexagonal in shape with the particle size in the range of 50–150 nm, see Fig. 1(a). The spherical VH_2 nanoparticles with a mean

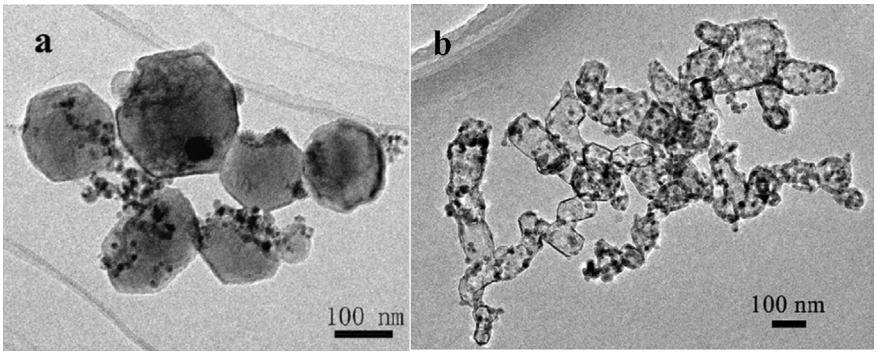

Fig. 1 – TEM bright-field images of the as-prepared Mg–V nanoparticles (a), the Mg–V nanoparticles after the hydrogen absorption under 4 MPa hydrogen pressure at 673 K (b) [60].

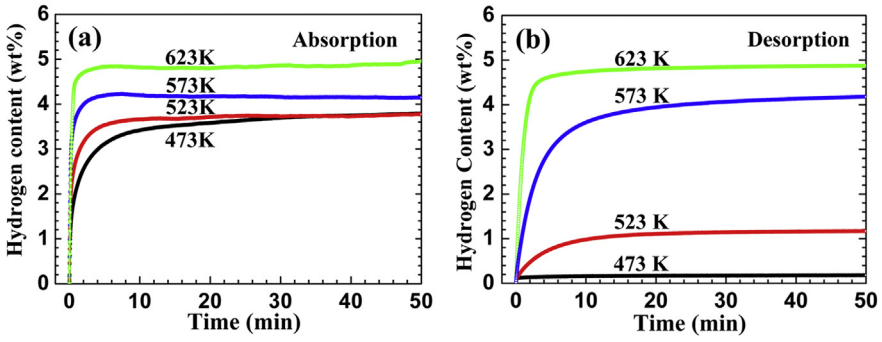

Fig. 2 – Hydrogen absorption curves under 4 MPa hydrogen pressure (a), and desorption curves under 100 Pa (b) of the Mg–V nanoparticles at 473, 523, 573 and 623 K [60].

diameter of 10 nm disperse evenly on the surface of the Mg nanoparticles. The formation of the Mg–V composite nanoparticles by HPMR and the hydrogen absorption and desorption processes can be summarized by the following equations, respectively:

$$Mg + V + H_2 \rightarrow Mg + MgH_2 + VH_2(\text{HPMR}) \quad (1)$$

$$Mg + V + H_2 \rightarrow MgH_2 + VH_2(\text{Absorption}) \quad (2)$$

$$MgH_2 + VH_2 \rightarrow Mg + V + H_2(\text{Desorption}) \quad (3)$$

After hydrogenation, the mean particle size of MgH_2 decreased to 60 nm, while the VH_2 nanoparticles were still about 10 nm, see Fig. 1(b). The Mg–V nanocomposite absorbed 3.8 wt.% hydrogen in less than 30 min at 473 K and accomplished a high storage capacity of 5.0 wt.% in less than 5 min at 623 K, see Fig. 2. This result was comparable with the very recent report that Mg nanoparticles with a mean particle size of 38 nm absorbed nearly 4 wt.% hydrogen in 40 min at 493 K [45]. Compared with the Mg nanoparticles of 38 nm, the Mg–V nanocomposite showed higher hydrogenation rate due to the catalytic effect of the V nanoparticles, especially at the initial stage. The Mg–V nanocomposite released 4.0 wt.% hydrogen in less than 15 min at 573 K. The catalytic effect of the V nanoparticles, and the nanostructure and the low oxide content of the Mg particles resulted in the low hydrogen absorption and desorption activation energies of 71.2 and 119.4 kJ mol^{-1}, respectively. It should be noted that the enhanced hydrogen sorption rate and storage capacity were due to the improved kinetics rather than the change in enthalpy.

Mg–Zn nanocomposite

Although different kinds of transition metals have been used as catalytic additives to enhance the hydrogen storage properties of Mg, the effect of Zn was rarely discussed. Deledda and coworkers [69] added Zn to Mg by ball milling in order to synthesize Mg–Zn intermetallic compounds. However, the final product was the amorphous Mg–Zn phase with a composition of $Mg_{45}Zn_{55}$. They further synthesized the Mg–Y–Zn ternary alloys and found that the phase transformations during hydrogen sorption were pressure dependent [70]. At pressures above 1 MPa, Mg_4Zn_7 decomposed into MgH_2 and $MgZn_2$. Since a large amount of Zn was added to Mg in these studies, the hydrogen storage capacity was reduced. Zn is one of elements, which can dissolve in hcp-Mg at the level of several mole percent. Moreover, on the basis of Mg–Zn binary diagram, Mg and Zn can form several kinds of intermetallics, such as MgZn, $MgZn_2$, Mg_2Zn_3 and Mg_2Zn_{11}. During the HPMR processing, the addition of Zn may modify the morphology and structure of Mg nanoparticles.

Liu et al. [61] synthesized the Mg-6.9 at.% Zn nanocomposite from the bulk Mg-10at.%Zn alloy by HPMR method. The particles were in spherical shape ranging from 100 to 700 nm with an average of about 400 nm. The XRD result proves that Zn partially dissolved in the α-Mg structure, see Fig. 3(a). A broad and diffusive peak between 40 and 43° indicates the formation of amorphous Mg–Zn phase during the solidification at very high cooling rate of 10^5 K/s in the HPMR processing. The amorphous Mg–Zn phase promoted the homogeneous growth of the composite particles into the spherical shape rather than the hexagonal shape of Mg. After the hydrogenation at 673 K, most of Mg in the Mg–Zn nanocomposite transformed into MgH_2, and the rest of the Mg combined with Zn to form intermetallics $MgZn_2$, see Fig. 3(b). After the desorption process, the Mg–Zn nanocomposite were broken into smaller particles with an average size of about 250 nm MgH_2 decomposed almost completely into the

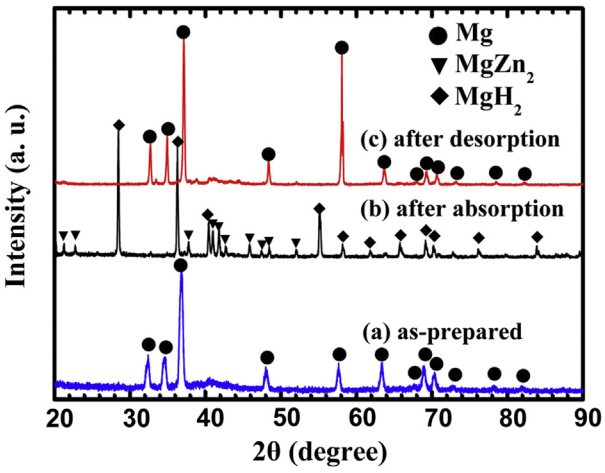

Fig. 3 – XRD patterns of the Mg–Zn nanocomposite, (a) as-prepared, (b) after the absorption in 4 MPa hydrogen at 673 K, and (c) after the desorption under 100 Pa at 673 K [61].

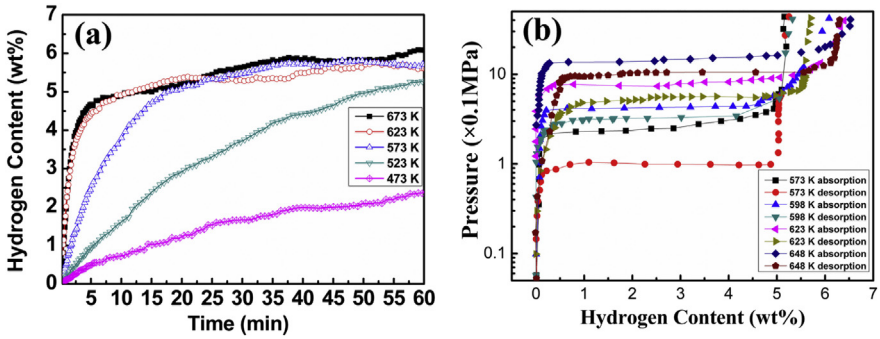

Fig. 4 – (a) Hydrogen absorption curves of the Mg–Zn nanocomposite at 473, 523, 573, 623 and 673 K under 4 MPa hydrogen pressure; (b) pressure-composition isotherm curves of the Mg–Zn nanocomposite at 573, 598, 623 and 648 K [61].

nanocrystalline α-Mg, and the intermetallics $MgZn_2$ transformed into the complex Mg–Zn intermetallics, see Fig. 3(c). The formation of Mg–Zn nanocomposite and the hydrogen absorption and desorption processes can be summarized by the following equations, respectively:

$$Mg + Zn \rightarrow Mg(Zn) + MgZn_x(\text{Amorphous}) \quad (4)$$

$$Mg(Zn) + MgZn_x(\text{Amorphous}) + H_2 \rightarrow MgH_2 + MgZn_2 \quad (5)$$

$$MgH_2 + MgZn_2 \rightarrow Mg(Zn) + MgZn_x(\text{Intermetallics}) \quad (6)$$

The addition of Zn played a crucial role in enhancing the sorption kinetics properties of the Mg–Zn nanocomposite. After one activation cycle, the Mg–Zn nanocomposite could absorb over 5.0 wt.% hydrogen in less than 20 min at 573 K, see Fig. 4(a). The presence of Mg–Zn alloy or intermetallics in the Mg–Zn nanocomposite may act as a catalyst to decrease the dissociation energy of H_2, leading to a low hydrogen absorption activation energy of 56.3 kJ mol^{-1}. The Mg–Zn nanocomposite could absorb 6.1 wt.% H_2 at 573 K, even though the addition of Zn deteriorated the hydrogen absorption capacity. The obtained value of the hydride formation enthalpy by the Van't Hoff plot for the Mg–Zn nanocomposite was −74.0 kJ mol^{-1}, similar with Mg, see Fig. 4(b).

Mg–Al nanocomposite

According to the discussion above, the Mg nanoparticles covered with metallic shell cannot be prepared in the Mg–Zn and Mg–V nanocomposites by HPMR. To reach the goal, a suitable Mg-based alloy should be designed. Among the alloying elements, Al is one of the most attractive candidates to decrease the stability of magnesium hydride. The hydrogen storage capacities of three Mg–Al intermetallic compounds, $Mg_{17}Al_{12}$, $Mg_{42}Al_{58}$ and Mg_2Al_3, are 4.44, 3.17, and 3.02 wt.%, respectively [71]. Wang and co-workers [72] reported that the ball-milled $Mg_{17}Al_{12}$ could absorb 2.19 wt.% hydrogen at 573 K in 40 min and the hydrogen desorption capacity reached 2.01 wt.% in 30 min at 613 K under hydrogen pressure of 0.1 MPa. It was reported recently that the hydrogen adsorption/desorption kinetics of Mg was significantly improved with Al addition, and the enthalpy of hydrogenation was decreased upon Al addition as the result of the endothermic disproportionate reactions of Mg–Al intermetallic compounds [71–74].

It is known that the stoichiometry compound nanoparticles can hardly form at very high cooling rate during the HPMR process, whereas the non-stoichiometry compounds with wide composition range are relatively easy to nucleate and grow into intermetallic compound nanoparticles. In the case of the Mg–Zn binary system with only stoichiometry compounds, the Mg–Zn intermetallics cannot be generated. As to the Mg–V system, the immiscible Mg and V nucleate in separate particles. The wide composition range of $Mg_{17}Al_{12}$ between 45 and 60.5 at.% Mg possibly enables its nucleation even at very high cooling rate. Recently, Liu et al. [62] successfully prepared the Mg-7, 22 and 27 at.% Al nanocomposites with $Mg@Mg_{17}Al_{12}$ structure from the Mg–Al alloy ingots by using HPMR method. With the addition of Al, the

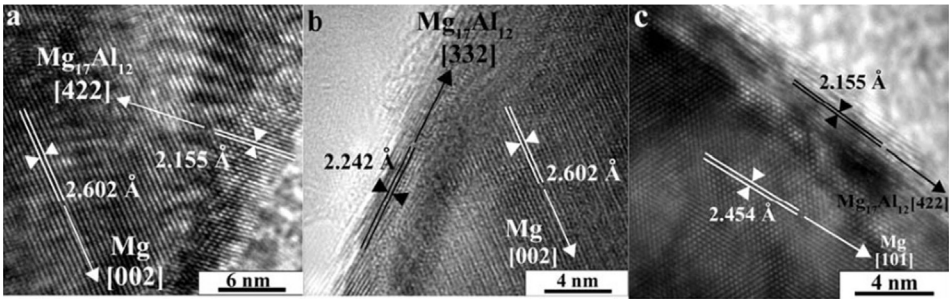

Fig. 5 – High resolution TEM images of the as-prepared Mg–Al nanocomposites: (a) Mg-7 at.% Al, (b) Mg-22 at.% Al and (c) Mg-27 at.% Al [62].

sizes of Mg–Al nanocomposites were effectively reduced to about 150 nm. The $Mg_{17}Al_{12}$ shell nucleated with the Mg core as a nucleation position, and the formation mechanism of the core/shell structure could be explained by the Mg–Al phase transformation. Surprisingly, no oxide phase was detected on the surface of these Mg–Al nanocomposites. The excellent oxidation resistance was ascribed to the fact that the $Mg_{17}Al_{12}$ shell in the Mg@$Mg_{17}Al_{12}$ nanocomposite provides much higher chemical stability than Mg. The thickness of $Mg_{17}Al_{12}$ shell increased from 2 to 3 nm for Mg-7 at.% Al to 4–5 nm for Mg-22 at.% Al, see Fig. 5. In order to control the content of $Mg_{17}Al_{12}$ in the nanocomposite, the content of Al should be adjusted. A high Al concentration, e.g. 27 at.% Al, led to the formation of fcc-Al and the reduced thickness of $Mg_{17}Al_{12}$.

The Mg@$Mg_{17}Al_{12}$ nanocomposites showed fast initial hydrogen absorption/desorption rates, and the hydrogen sorption kinetics and storage capacity decreased with the increasing Al concentration. Mg-7 at.% Al nanocomposite absorbed 3.3 wt.% H_2 at 473 K in 60 min, as shown in Fig. 6(a). This result was comparable with the Mg nanocomposite of 38 nm [45], but was superior to that of the Mg–Zn nanocomposite that absorbed 2.3 wt.% H in 60 min at 473 K [61]. It is surprising to find that the hydrogen storage capacity of Mg-7 at.% Al nanocomposite was as high as 5.7 wt.% at 523 K. The storage capacity reached 6.2 wt.% H_2 at 573 K. As compared to the Mg nanocomposite embedded in a gas-selective polymer matrix of about 40 wt.%, which had a storage capacity of 4 wt.% [53], the thin $Mg_{17}Al_{12}$ shell of 2–3 nm not only prevents the Mg nanocomposites from oxidation, but also offers a high hydrogen storage capacity of nearly 7.0 wt.% at 673 K, only about 10% less than the theoretical gravimetric capacity of MgH_2. It is noted that the Mg@$Mg_{17}Al_{12}$ nanocomposite released 6.0 wt.% H_2 within 30 min at 623 K, and 6.2 wt.% H_2 within 3 min at 673 K, see Fig. 6(b). The $Mg_{17}Al_{12}$ shell disproportionated into MgH_2 and Al upon hydrogenation, and was recovered after the hydrogen release. The recovery of $Mg_{17}Al_{12}$ is of great importance for sustaining the excellent hydrogen storage reversibility. The morphology and size of the nanocomposite was not apparently changed during the hydrogenation/dehydrogenation cycle, whereas the particle core Mg changed from single crystal into polycrystalline of 2–4 nm. The whole hydrogenation process of the Mg@$Mg_{17}Al_{12}$ nanocomposite can be expressed as follows:

$$Mg + Mg_{17}Al_{12} + H_2 \rightarrow Al + MgH_2 \quad (7)$$

The hydrogen desorption process of the Mg@$Mg_{17}Al_{12}$ nanocomposite can be formulized as follows:

$$Al + MgH_2 \rightarrow Mg + Al + H_2 \rightarrow Mg + Mg_{17}Al_{12} + H_2 \quad (8)$$

The calculated E_a value for the hydrogen absorption of Mg@$Mg_{17}Al_{12}$ nanocomposite is 49.3 kJ mol^{-1}, lower than that of the magnesium thin film of 72 kJ mol^{-1} [75], and much lower than that of the Mg in 38 nm of 115 kJ mol^{-1} [45]. The calculated hydrogen desorption activation energy is 105.5 kJ mol^{-1}, which is also lower than that of the Mg in 38 nm of 126 kJ mol^{-1} [45]. Thus, the high hydrogen sorption rate is attributed to the catalytic effect and oxidation resistance of the $Mg_{17}Al_{12}$ shell, and the nanostructure of the Mg particle core. The Mg@$Mg_{17}Al_{12}$ nanocomposite with high hydrogen sorption rate, high hydrogen storage capacity and low operation temperature, is promising for the application as a hydrogen storage material.

Mg–La–Al and Mg–La–Ni nanocomposites

In order to clarify whether Mg-based ternary system can form core/shell structure nanocomposite, Liu et al. [63,64] further produced the Mg-2 at.%La-2.6 at.%Al and the Mg-10.6 wt.% La-3.5 wt.% Ni nanocomposites by HPMR method. However, no metallic shell can be found in both Mg–La–Al and Mg–La–Ni systems. For the Mg–La–Al nanocomposite, these nanoparticles are made of single crystalline Mg of about 160 nm, and a little amount of polycrystalline Al_2La of 15 nm dispersing on the surface of Mg. After hydrogenation, Al_2La disproportionates into single crystalline LaH_3 of 15 nm. As to the Mg–La–Ni system, these nanoparticles were made of Mg, LaH_3 and a small amount of Mg_2Ni. LaH_3 and Mg_2Ni nanoparticles were nearly spherical in shape with the mean particle size of 15 nm, and dispersed on the surface of Mg (180 nm). The hydrogen storage properties of both nanocomposites have been improved remarkably. The Mg–La–Al nanocomposite can absorb 5.0 wt.% H_2 in 30 min at 473 K, and the storage capacity is as high as 6.8 wt.% at 673 K. It can also release 6.0 wt.% H_2 in less than 10 min at 673 K. The Mg–La–Ni nanocomposite also accomplished a hydrogen storage capacity of 6.5 wt.% H_2 in less than 10 min at 673 K. The

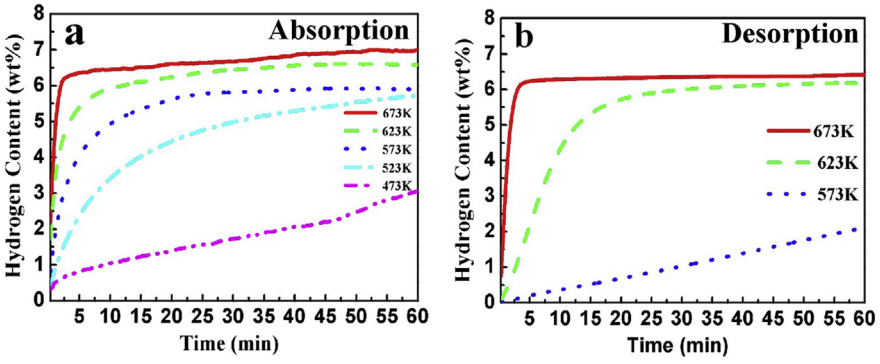

Fig. 6 – Hydrogen absorption curves of the Mg-7 at.% Al nanocomposite at 473, 523, 573, 623 and 673 K under 4 MPa (a), and desorption curves at 573, 623 and 673 K under 100 Pa [62].

catalytic effect of LaH_3 and Mg_2Ni nanoparticles promoted the hydrogen sorption process.

Mg-based nanocomposite prepared by RS technique

Ball milling generally results in the reduced grain size and formation of various defects [76]. In addition to ball milling, RS through melt-spun is also an effective way to obtain the Mg-based nanocomposites. The hydrogen storage capacity and hydrogenation/absorption kinetics of the Mg-based nanocomposites were influenced by a number of factors, including chemical composition, microstructure and grain size. Compared to the conventional Mg-based alloys with micrometer crystalline, the nanocrystalline Mg combined with other catalysts in nanoscale exhibit much faster rate of hydrogen absorption/desorption and lower temperature of hydrogenation/dehydrogenation [77,79]. The large number of interfaces and grain boundaries available in nanocrystalline materials provides easy pathways for hydrogen diffusion and promotes the absorption of hydrogen. Spassov et al. [77,78] studied the hydrogen storage properties and thermal stability of Mg–Ni–RE nanocomposite (RE = Y, La, Ce) with nanocrystalline and amorphous or partially amorphous microstructures, and reported that the difference in the hydrogenation properties between the as-quenched nanocrystalline/amorphous and completely nanocrystalline was insignificant. Huang et al. [79] studied the nanocrystallization and hydrogenation properties of amorphous $Mg_{65}Cu_{25}Nd_{10}$ prepared by melt-spinning. They found that $Mg_{65}Cu_{25}Nd_{10}$ nanocomposite showed fast initial hydrogenation rate and high hydrogen capacity.

Wu et al. [80,81] obtained Mg-based Mg–20Ni–8Mm (wt.%) (Mm = Ce, La-rich Mischmetal) nanocomposite with microcrystalline, nanocrystalline, and amorphous microstructures by controlling the solidification rate of the melt-spun ribbon. The microstructure was remarkably refined by rapid solidification compared with that of the conventional polycrystalline alloy, see Fig. 7. A considerable amount of nanocrystalline Mg and Mg_2Ni was produced in the amorphous matrix. Mischmetal-containing $Mg_{12}Mm$ intermetallic precipitated preferentially at the boundary of magnesium grains, providing additional pathways for hydrogen diffusion into the Mg. The hydrogen absorption kinetics was improved in the order "Cu-300 < Cu-1000 < Cu-2000" (the numbers denote the spinning velocity of the copper wheel in rpm) [81]. During the hydrogenation, the grain refinement of the Mg–Ni–Mm alloy introduced by the RS process resulted in the formation of Mg_2NiH_4 and the solid solution hydride $Mg_2NiH_{0.3}$, and the decrease in the unit cell volumes of the constituent hydride phases. This was explained by the increased mechanical stresses in the materials and/or by the increased interfacial energy of the fine grains of the corresponding hydrides. The temperature range of dehydrogenation from the hydrogenated alloys decreased in the order "Cu-300 > Cu-1000 >> Cu-2000", which was explained by the increased uniformity of the hydrides grain size with the increasing solidification rate. During PCT (pressure composition temperature) tests, see Fig. 8, the Cu-1000 and Cu-2000 samples displayed not only larger pressure hysteresis and smaller slope of the plateau, but also lower hydrogen storage capacity.

Wu et al. [82] also studied the microstructure and hydrogen storage properties of the melt-spun Mg–10Ni–2Mm (at.%) nanocomposite. By increasing the solidification rate, the kinetics of the H-absorption/desorption reactions of the melt-spun ribbons was greatly improved due to the grain

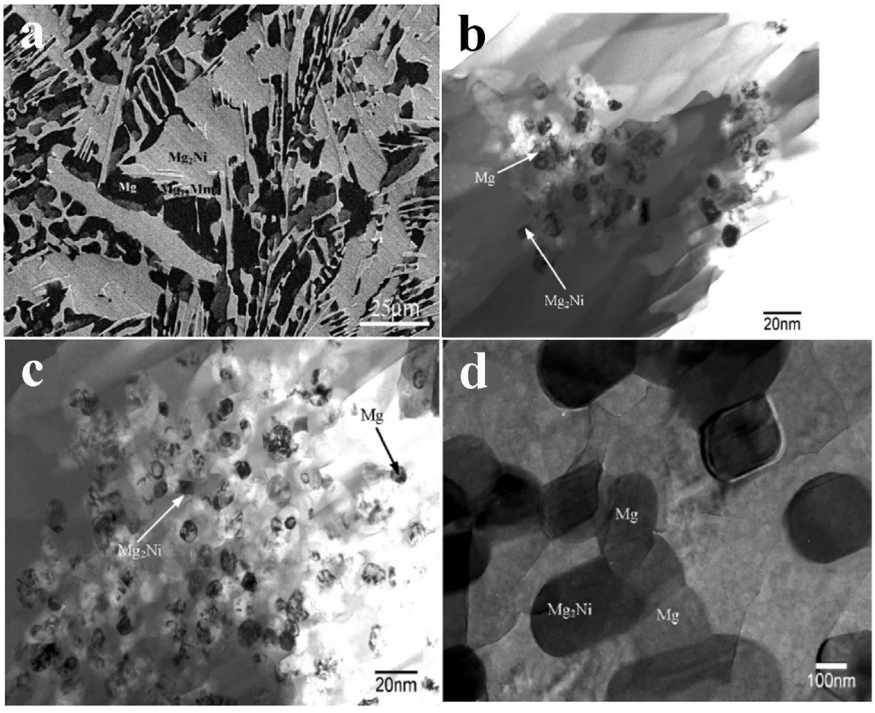

Fig. 7 – SEM micrograph of the as-cast Mg–20Ni–8Mm alloy (a), and TEM micrographs of the melt-spun Mg–20Ni–8Mm alloy at the copper wheel velocity of 20.9 m s^{-1} (b), 10.5 m s^{-1} (c), 3.1 m s^{-1} (d) [80].

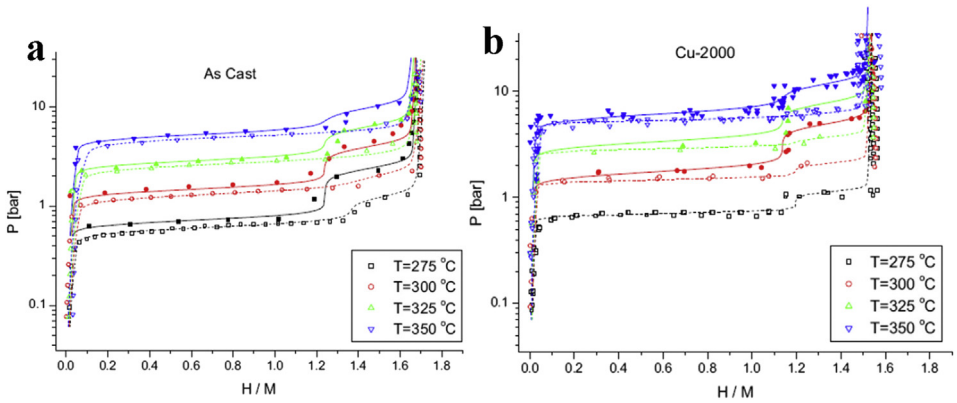

Fig. 8 – Measured (points) and calculated (lines) hydrogen absorption (filled symbols, solid lines) and desorption (empty symbols, dot lines) PCT isotherms for the as-cast and melt-spun Mg–Ni–Mm under 2.5 MPa hydrogen pressure [81].

refinement and the formation of nanocrystallines from amorphous phase. RS processing resulted in the formation of Mg_2NiH_4 and the solid solution hydride phase $Mg_2NiH_{0.3}$ due to incomplete hydrogenation of Mg_2Ni. The maximum hydrogen storage capacity of the melt-spun ribbons depended on the contents of different hydrides. At various solidification rate, the hydrogen storage capacities were 5.1, 4.6 and 4.2 wt.% H_2 for the Cu-300, Cu-1000 and Cu-2000 samples, respectively. Vacuum TDS gave a much narrower desorption temperature range (220–330 °C, peak at 286 °C) for the Cu-2000 sample than that for the Cu-1000 (210–395 °C, peak at 294 °C), due to the increased uniformity of the hydride particle size with the increasing solidification rate.

Wu et al. further compared the microstructure and hydrogen storage properties of the melt-spun Mg–10Ni–2Mm (at.%) nanocomposites with those of the ball-milled sample [83]. The melt-spun ribbon alloy and the 2 h ball-milled alloy reached a maximum hydrogen storage capacity of 4.2 wt.% in 141 min and 3.2 wt.% in 210 min, respectively. Vacuum TDS of the melt-spun alloy showed narrower desorption temperature range (220–330 °C) than the ball-milled one (250–425 °C). The types of hydrides were closely related to the microstructure. TEM micrographs demonstrated that the grains remained in nanoscale in the melt-spun ribbons even after annealing at 350 °C during cycles, see Fig. 9. This proves that the RS technique is an effective way to obtain Mg-based nanocomposite with improved hydrogen storage properties. According to the results of Orimo and Fujii [84], the hydrogen concentration at the grain boundary is much higher than that at the grain interior region and amorphous region. The formation of nanocrystalline increases the grain boundary in the melt-spun ribbon, which promotes the hydrogen storage properties.

TEM studies of the as-quenched ribbons and ball-milled hydrides of the Mg–10Ni–2Mm alloy showed the refinement of the microstructures during the processing and the nucleation of $MmMg_{12}$ intermetallic at the grain boundaries of Mg and Mg_2Ni, see Fig. 10 [85]. The interface between $MmMg_{12}$ and Mg_2Ni was semi-coherent, with an ordered repetition of the consistent atomic arrangements. The kinetics of H-absorption/desorption was improved due to the fast hydrogen diffusion in the nanograins, thus, providing paths for H-exchange. The nano-sized grains in the ball-milled Cu-1000 sample were stable during the cycling of hydrogen desorption and absorption at 350 °C, and MmH_{3-x} was derived from $MmMg_{12}$ at grain boundaries of MgH_2, see Fig. 11. MmH_{3-x} and Mg_2NiH_4 acted as the nucleation centers to initiate the formation of MgH_2, promoting the hydrogen absorption of Mg. PCT diagrams showed two plateaus of Mg–MgH_2 and Mg_2Ni–Mg_2NiH_4, see Fig. 11. The MgH_2 plateau exhibited no hysteresis and practically no slope, while the plateau of Mg_2NiH_4 exhibited a pronounced hysteresis and a slope, particularly for the nanocomposite. The maximum hydrogen storage capacity of the nanocomposite was higher than that of the microcrystalline one.

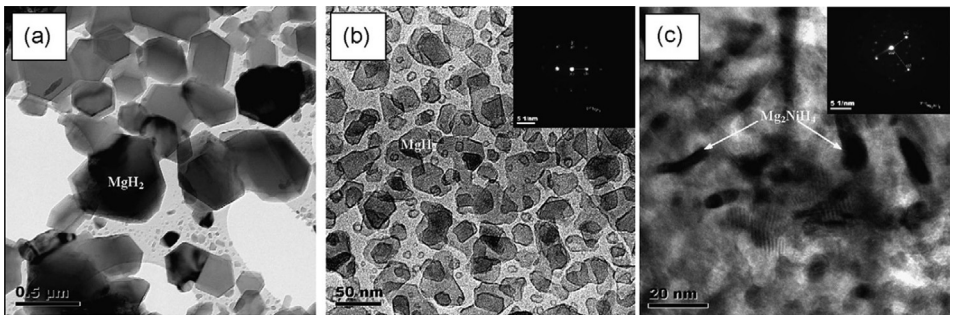

Fig. 9 – TEM micrographs of the coarse grains of MgH_2 in the 2 h ball-milled Mg–10Ni–2Mm alloy (a), the nanograins of MgH_2 (b), and the Mg_2NiH_4 hydrides in the melt-spun Mg–10Ni–2Mm ribbon (c) [83].

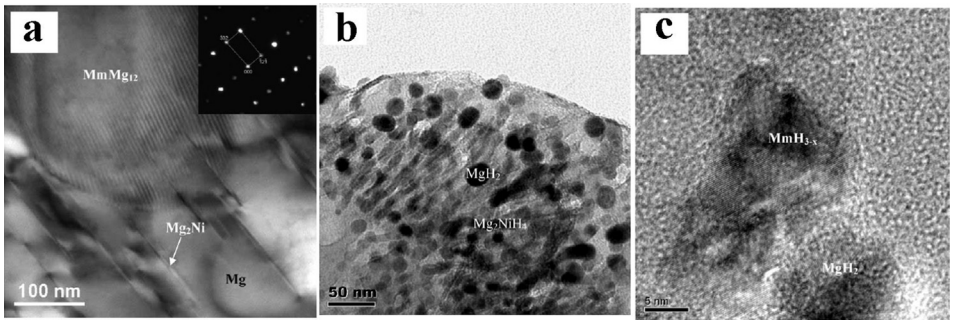

Fig. 10 – High resolution TEM micrograph of the melt-spun Mg–10Ni–2Mm solidified with a copper wheel surface velocity of 3.1 m s^{-1} (a), TEM micrograph of the ball-milled Cu-1000 Mg–10Ni–2Mm ribbon after 3 cycles of hydrogen desorption–hydrogenation (b), and high resolution TEM of MmH_{3-x} phase at the grain boundary of the MgH_2 (c) [85].

Mg-based nanocomposite synthesized by other methods

The Mg-based nanocomposites have also been synthesized through nanoconfinement, especially combining with the carbon materials to stabilize Mg nanoparticles over hydrogen uptake and release cycles. Carbonaceous materials are often selected as the most suitable scaffold materials due to their lightweight, chemically inert, good thermal conductivity and mechanically flexible to withstand repeated volume change [53,86–89]. Jongh et al. [53] synthesized the Mg nanoparticles of several nanometers by melt infiltration of nanoporous carbon with Mg, and most of the Mg nanoparticles were not oxidized. However, these composites contained only 10–15 wt.% Mg due to the large quantity of carbon, which was difficulty to be removed. Gross et al. [90] used a similar approach to synthesize MgH_2 nanoparticles of 2–30 nm confined in a porous carbon host. This nanocomposite can release about 5 mass% hydrogen at 250 °C due to the fine particle size and catalytic effect of Cu and Ni from the wetting layers. Nevertheless, the thermodynamics change was not observed in this nanocomposite.

More recently, Jeon et al. [54] reported the synthesis of air-stable Mg nanocomposite by encapsulation of 5–15 nm Mg in polymer poly (methylmetha-crylate). The polymer effectively protected the Mg nanoparticles from O_2 and H_2O, and the nanocomposite showed stability after two weeks of air exposure. Moreover, the polymer matrix was gas-selective, which enabled Mg nanoparticles to absorb and release hydrogen at a rapid rate without being oxidized. Even without any catalysts, the nanocomposite displayed a fast hydrogenation kinetics and possessed a storage capacity of 4 wt.% H_2 at 200 °C in 30 min, see Fig. 12. Theoretical modeling indicated that the hydrogenation of Mg nanocomposite carried out through 1D growth, namely along line defects. The hydrogen storage capacity of this nanocomposite can be further increased if the matrix polymer content is reduced.

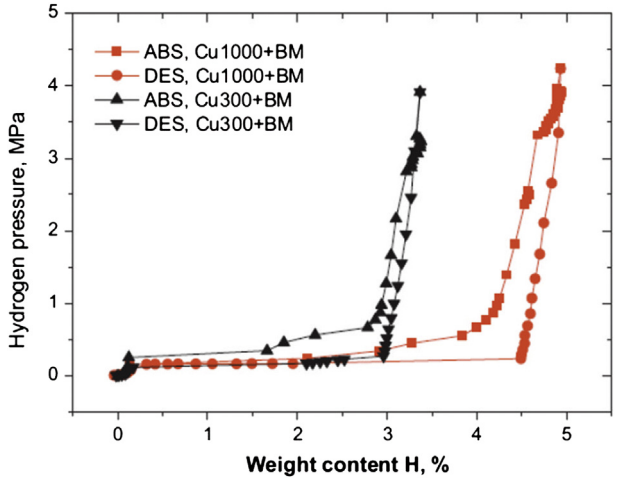

Fig. 11 – PCT absorption and desorption isotherms for the ball-milled Mg–10Ni–2Mm ribbon at 300 °C [85].

The Mg-based nanocomposites of thin film have been prepared by magnetron sputtering method, and their chemical composition, dimension and crystallinity can be accurately tailored in nanoscale by adjusting the power of the targets [91–96]. Various elements have been added into the Mg-based thin film to produce multilayer nanocomposites and improve their hydrogen storage properties. Bendersky and co-workers demonstrated that the hydrogenation kinetics of Mg-4 at.% Fe films was enhanced in comparison to pure Mg [91]. Xin et al. prepared Mg/Ti/Pd trilayer films and found that the hydrogen storage properties of Mg/Pd films could be significantly improved with the addition of a Ti interlayer [92]. Ouyang and coworkers proved that the hydrogen absorption content of MgNi/Pd multilayer thin films deposited using MgNi alloy target reached to 4.6 mass% at room temperature and hydrogen desorption reached 3.4 mass% hydrogen [93]. Mitlin et al. reported that the Mg–Fe–Ti films were capable of absorbing nearly 5 wt.% hydrogen in seconds and desorbing in minutes, and this sorption behavior was stable over cycling [94]. They further investigated the Mg–AlTi multilayers with 2 nm thick AlTi layer, and found that these nanocomposites accomplished a hydrogen capacity of 5.1 wt.% at 473 K without significant degradation over 200 cycles [95]. Moreover, the rapid sorption kinetics and microstructure stability can be maintained over 250 cycles. Recently, Liu et al. prepared the Mg_xNi_{100-x}/Pd films by magnetron co-sputtering Mg and Ni targets with a Pd layer of 10 nm deposited on these films [96]. Mg_2Ni and $MgNi_2$ are

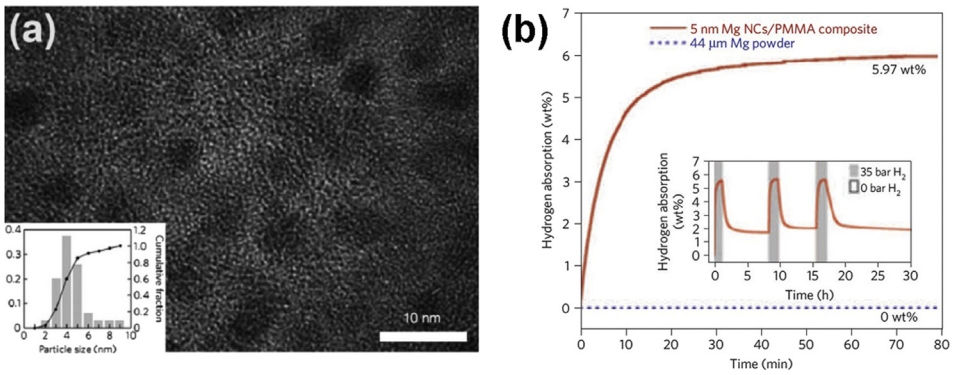

Fig. 12 – (a) TEM image and (b) the hydrogenation/dehydrogenation properties of the Mg/PMMA nanocomposites [54].

directly generated during the co-sputtering process in the $Mg_{84}Ni_{16}$/Pd and $Mg_{48}Ni_{52}$/Pd films. The hydrogenation of the $Mg_{84}Ni_{16}$/Pd film saturates within 45 s under 0.1 MPa H_2 at 298 K and exhibits the fastest absorption kinetics compared with the $Mg_{94}Ni_6$/Pd and $Mg_{48}Ni_{52}$/Pd films. The maximum discharge capacity of the $Mg_{84}Ni_{16}$/Pd film carried out in 6 M KOH with a three-electrode cell is as high as 482.7 mA h g^{-1}.

Conclusions

To realize the hydrogen economy, the development of a safe and efficient hydrogen storage approach is the key issue. Recent achievements in the Mg-based hydrogen storage materials have shown the possibility to overcome their disadvantages of unfavorable thermodynamics and poor kinetics. Optimization of the composition of Mg-based alloys, in combination with the mechano-chemical treatment accelerates the hydrogen absorption/desorption rates at much moderate conditions. However, because of thermodynamic limitation, the hydrogen desorption still requires rather high temperature.

Many strategies have been adopted within the past decade to improve the hydrogen storage properties of the Mg-based materials, including modifying microstructure by ball milling, alloying with other elements, doping with catalysts, and nanosizing. To further improve the hydrogen storage properties, the Mg nanoparticle or nanocrystalline is combined with other materials to form nanocomposite. The Mg-based nanocomposites produced by HPMR, RS technique, and other approaches, effectively enhance the sorption kinetics of Mg by facilitating hydrogen dissociation and diffusion, and prevent particle sintering and grain growth of Mg during hydrogenation/dehydrogenation process. However, it is still quite challenging for these nanocomposites to absorb/desorb hydrogen below 373 K. Novel Mg-based nanocomposites, which not only confine Mg nanoparticles but also catalyze the sorption processing, are required. To achieve this goal, new theories for designing nanocomposites and the state of art technologies for synthesizing the nanocomposites are highly needed. Further progress in materials science would most probably result in the development of new weight efficient hydrogen storage materials based on magnesium.

Acknowledgments

The authors acknowledge the support of this work by MOST of China (No. 2011AA03A408), the National Natural Science Foundation of China (Grant No. 51371056), the Aeronautical Science Foundation of China (No. 2011ZF51065), China Program of Magnetic Confinement Fusion under grant number 2012GB102006 and the Scientific Research Foundation for the Returned Overseas Chinese Scholars, State Education Ministry.

REFERENCES

[1] DOE: US Department of Energy. Website: http://www.doe.gov.
[2] Sakintuna B, Lamari-Darkrim F, Hirscher M. Metal hydride materials for solid hydrogen storage: a review. Int J Hydrogen Energy 2007;32:1121–40.
[3] Demircan A, Demiralp M, Kaplan Y, Mat MD, Veziroglu TN. Experimental and theoretical analysis of hydrogen absorption in $LaNi_5$–H_2 reactors. Int J Hydrogen Energy 2005;30:1437–46.
[4] Simičić MV, Zdujić M, Dimitrijević R, Nikolić-Bujanović L, Popović NH. Hydrogen absorption and electrochemical properties of Mg_2Ni-type alloys synthesized by mechanical alloying. J Power Sources 2006;158:730–4.
[5] Orimo SI, Nakamori Y, Eliseo JR, Züttel A, Jensen CM. Complex hydrides for hydrogen storage. Chem Rev 2007;107:4111–32.
[6] Chen P, Xiong Z, Luo J, Lin J, Tan KL. Interaction of hydrogen with metal nitrides and imides. Nature 2002;420:302–4.
[7] Wu H, Zhou W, Pinkerton FE, Meyer MS, Srinivas G, Yildirim T, et al. A new family of metalborohydride ammonia borane complexes: synthesis, structures, and hydrogen storage properties. J Mater Chem 2010;20:6550–6.
[8] Mushnikov NV, Ermakov AE, Uimin MA, Gaviko VS, Terentev PB, Skripov AV, et al. Kinetics of interaction of Mg-based mechanically activated alloys with hydrogen. Phys Met Metall 2006;102(4):421–31.
[9] Andreasen A, Vegge T, Pedersen AS. Compensation effect in the hydrogenation/dehydrogenation kinetics of metal hydrides. J Phys Chem B 2005;109:3340–4.
[10] Zaluska A, Zaluski L, Strom-Olsen JO. Nanocrystalline magnesium for hydrogen storage. J Alloys Compd 1999;288:217–25.

[11] Schlapbach L, Shaltiel D, Oelhafen P. Catalytic effect in the hydrogenation of Mg and Mg compounds: surface analysis of Mg–Mg_2Ni and Mg_2Ni. Mater Res Bull 1979;14:1235–46.

[12] Sholl DS. Using density functional theory to study hydrogen diffusion in metals: a brief overview. J Alloys Compd 2007;446:462–8.

[13] Segal VM, Reznikov VI, Drobyshevskiy AE, Kopylov VI. Plastic working of metals by simple shear. Russ Metall 1981;1:99–105.

[14] Yao X, Zhu ZH, Cheng HM, Lu GQ. Hydrogen diffusion and effect of grain size on hydrogenation kinetics in magnesium hydrides. J Mater Res 2008;23:336–40.

[15] Vigeholm B, Kjoller J, Larsen B, Pedersen AS. Formation and decomposition of magnesium hydride. J Less Common Met 1983;89:135–44.

[16] Berube V, Radtke G, Dresselhaus M, Chen G. Size effects on the hydrogen storage properties of nanostructured metal hydrides: a review. Int J Energy Res 2007;31:637–63.

[17] Shang C, Guo ZX. Structural and desorption characterisations of milled (MgH_2 t Y, Ce) powder mixtures for hydrogen storage. Int J Hydrogen Energy 2007;32(4):2920–5.

[18] Guoxian L, Erde W, Shoushi F. Hydrogen absorption and desorption characteristics of mechanically milled Mg–35 wt % $FeTi_{1.2}$ powders. J Alloys Compds 1995;223:111–4.

[19] Huot J, Akiba E, Takasa T. Mechanical alloying of Mg–Ni compounds under hydrogen and inert atmosphere. J Alloys Compds 1995;231:815–9.

[20] Zaluski L, Zaluska A, Strom–Olsen JO. Nanocrystalline metal hydrides. J Alloys Compds 1997;253–254:70–9.

[21] Shao H, Asano K, Enoki H, Akiba E. Fabrication and hydrogen storage property study of nanostructured Mg–Ni–B ternary alloys. J Alloys Compd 2009;479:409–13.

[22] Shao HY, Asano K, Enoki H, Akiba E. Preparation and hydrogen storage properties of nanostructured Mg–Ni BCC alloys. J Alloys Compd 2009;477:301–6.

[23] Kim H, Nakamura J, Shao HY, Nakamura Y, Akiba E, Chapman KW. Insight into the hydrogenation properties of mechanically alloyed $Mg_{50}Co_{50}$ from the local structure. J Phys Chem C 2011;115:20335–41.

[24] Shao H, Asano K, Enoki H, Akiba E. Fabrication, hydrogen storage properties and mechanistic study of nanostructured $Mg_{50}Co_{50}$ body-centered cubic alloy. Scr Mater 2009;60:818–21.

[25] Reilly JJ, Wiswall RH. Reaction hydrogen with alloys magnesium and nickel and formation of Mg_2NiH_4. Inorg Chem 1968;7:2254.

[26] Pozzo M, Alfe D. Structural properties and enthalpy of formation of magnesium hydride from quantum Monte Carlo calculations. Phys Rev B 2008;77:104103.

[27] Zhang Y, Tsushio Y, Enoki H, Akiba E. The study on binary Mg–Co hydrogen storage alloys with BCC phase. J Alloys Compds 2005;393:147–53.

[28] Matsuda J, Shao H, Nakamura Y, Akiba E. The nanostructure and hydrogenation reaction of $Mg_{50}Co_{50}$ BCC alloy prepared by ball-milling. Nanotechnology 2009;20:204015.

[29] Shao HY, Liu T, Wang YT, Xu HR, Li XG. Preparation of Mg-based hydrogen storage materials from metal nanoparticles. J Alloys Compds 2008;465:527–33.

[30] Liu T, Shen HL, Liu Y, Xie L, Qu JL, Shao HY, et al. Scaled-up synthesis of nanostructured Mg-based compounds and their hydrogen storage properties. J Power Sources 2013;227:86–93.

[31] Hanada N, Ichikawa T, Fujii JH. Catalytic effect of nanoparticle 3d-Transition metals on hydrogen storage properties in magnesium hydride MgH_2 prepared by mechanical milling. J Phys Chem B 2005;109:7188–94.

[32] Lu J, Choi YJ, Fang ZZ, Sohn HY, Ronnebro E. Hydrogen storage properties of nanosized MgH_2–$0.1TiH_2$ prepared by ultrahigh-energy-high-pressure milling. J Am Chem Soc 2009;131:15843–52.

[33] Varin RA, Zaranski Z, Czujko T, Polanski M, Wronski ZS. The composites of magnesium hydride and iron-titanium intermetallic. Int J Hydrogen Energy 2011;36:1177–83.

[34] Dolci F, Chio MD, Baricco M, Giamello E. The interaction of hydrogen with oxidic promoters of hydrogen storage in magnesium hydride. Mater Res Bull 2009;44:194–7.

[35] Malka IE, Czujko T, Bystrzycki J. Catalytic effect of halide additives ball milled with magnesium hydride. Int J Hydrogen Energy 2010;35:1706–12.

[36] Fu Y, Groll M, Mertz R, Kulenovic R. Effect of $LaNi_5$ and additional catalysts on hydrogen storage properties of Mg. J Alloys Compd 2008;460:607–13.

[37] Makihara Y, Umeda K, Shoji F, Kato K, Miyairi Y. Cooperative dehydriding mechanism in a mechanically milled Mg-50mass% $ZrMn_2$ composite. J Alloys Compd 2008;455:385–91.

[38] Vijay R, Sundaresan R, Maiya MP, Murthy SS, Fu Y, Klein HP. Characterization of Mg-x wt% FeTi ($x = 5$–30) and Mg-40 wt% FeTiMn hydrogen absorbing materials prepared by mechanical alloying. J Alloys Compd 2004;384:283–95.

[39] Hanada N, Ichikawa T, Hino S, Fujii H. Remarkable improvement of hydrogen sorption kinetics in magnesium catalyzed with Nb_2O_5. J Alloys Compd 2006;420:46–9.

[40] Wagemans RWP, van Lenthe JH, de Jongh PE, van Dillen AJ, de Jong KP. Hydrogen storage in magnesium clusters: quantum chemical study. J Am Chem Soc 2005;127:16675–80.

[41] Jongh PE, Adelhelm P. Nanosizing and nanoconfinement: new strategies towards meeting hydrogen storage goals. Chem Sus Chem 2010;3:1332–48.

[42] Arrowsmith M, Hill MS, MacDougall DJ, Mahon MF. A hydride-rich magnesium cluster. Angew Chem Int Ed 2009;48:4013–6.

[43] Harder S, Spielmann J, Intemann J, Bandmann H. Hydrogen storage in magnesium hydride: the molecular approach. Angew Chem Int Ed 2011;50:4156–60.

[44] Aguey-Zinsou KF, Ares-Fern JR. Synthesis of colloidal magnesium: a near room temperature store for hydrogen. Chem Mater 2008;20:376–8.

[45] Norberg NS, Arthur TS, Fredrick SJ, Prieto AL. Size-dependent hydrogen storage properties of Mg nanocrystals prepared from solution. J Am Chem Soc 2011;133:10679–81.

[46] Haas I, Gedanken A. Synthesis of metallic magnesium nanoparticles by sonoelectrochemistry. Chem Commun; 2008:1795–7.

[47] Li W, Li C, Ma H, Chen J. Magnesium nanowires: enhanced kinetics for hydrogen absorption and desorption. J Am Chem Soc 2007;129:6710–1.

[48] Barcelo S, Rogers M, Grigoropoulos CP, Mao SS. Hydrogen storage property of sandwiched magnesium hydride nanoparticle thin film. Int J Hydrogen Energy 2010;35:7232–5.

[49] Cheng FY, Tao ZL, Liang J, Chen J. Efficient hydrogen storage with the combination of lightweight Mg/MgH_2 and nanostructures. Chem Commun 2012;48:7334–43.

[50] Dehouche Z, Djaozandry R, Huot J, Boily S, Goyette J, Bose TK, et al. Influence of cycling on the thermodynamic and structure properties of nanocrystalline magnesium based hydride. J Alloys Compd 2000;305:264–71.

[51] Kyoi D, Sato T, Rönnebro E, Kitamura N, Ueda A, Ito M. A new ternary magnesium–titanium hydride Mg_7TiH_x with hydrogen desorption properties better than both binary magnesium and titanium hydrides. J Alloys Compd 2004;372:213–7.

[52] Chaise A, de Rango P, Marty P, Fruchart D. Experimental and numerical study of a magnesium hydride tank. Int J Hydrogen Energy 2010;35:6311–22.
[53] de Jongh PE, Wagemans RWP, Eggenhuisen TM, Dauvillier BS, Radstake PB, Meeldijk JD, et al. The preparation of carbon-supported magnesium nanoparticles using melt infiltration. Chem Mater 2007;19:6052–7.
[54] Jeon KJ, Moon HR, Ruminski AM, Jiang B, Kisielowski C, Bardhan R, et al. Air-stable magnesium nanocomposites provide rapid and high-capacity hydrogen storage without using heavy-metal catalysts. Nat Mater 2011;10:286–90.
[55] Krishnan G, Palasantzas G, Kooi BJ. Influence of Ti on the formation and stability of gas-phase Mg nanoparticles. Appl Phys Lett 2010;97:261912.
[56] Krishnan G, Palasantzas G, Kooi BJ. Improved thermal stability of gas-phase Mg nanoparticles for hydrogen storage. Appl Phys Lett 2010;97:131911.
[57] Li XG, Chiba A, Takahashi S. Preparation and magnetic properties of ultrafine particles of Fe–Ni alloys. J Magn Magn Mater 1997;170:339–45.
[58] Liu T, Shao HY, Li XG. Synthesis and characteristics of Ti–Fe nanoparticles by hydrogen plasma-metal reaction. Intermetallics 2004;12:97–102.
[59] Liu T, Shao HY, Li XG. Oxidation behavior of Fe_3Al nanoparticles. Nanotechnology 2003;14:542–5.
[60] Liu T, Zhang TW, Qin CG, Zhu M, Li XG. Improved hydrogen storage properties of Mg–V nanoparticles prepared by hydrogen plasma–metal reaction. J Power Sources 2011;196:9599–604.
[61] Liu T, Zhang TW, Zhang XZ, Li XG. Synthesis and hydrogen storage properties of ultrafine Mg–Zn particles. Int J Hydrogen Energy 2011;36:3515–20.
[62] Liu T, Qin CG, Zhang TW, Cao YR, Zhu M, Li XG. Synthesis of $Mg@Mg_{17}Al_{12}$ ultrafine particles with superior hydrogen storage properties by hydrogen plasma–metal reaction. J Mater Chem 2012;22:19831.
[63] Liu T, Qin CG, Zhu M, Cao YR, Shen HL, Li XG. Synthesis and hydrogen storage properties of Mg–La–Al nanoparticles. J Power Sources 2012;219:100–5.
[64] Liu T, Cao YR, Qin CG, Li XG. Synthesis and hydrogen storage properties of Mg–10.6La–3.5Ni nanoparticles. J Power Sources 2014;246:277–82.
[65] Cummings DL, Powers GJ. The storage of hydrogen as metal hydrides. Ind Eng Chem Process Des Dev 1974;13:182–92.
[66] Liang G, Huot J, Boily S, Neste AV, Schulz R. Catalytic effect of transition metals on hydrogen sorption in nanocrystalline ball milled MgH_2–Tm (Tm = Ti, V, Mn, Fe and Ni) systems. J Alloys Compd 1999;292:247–52.
[67] Kondo T, Sakurai Y. Hydrogen absorption–desorption properties of Mg–Ca–V BCC alloy prepared by mechanical alloying. J Alloys Compd 2006;417:164–8.
[68] Smith JF, Lee KJ. In: Massalski TB, editor. Binary alloy phase diagrams. 2nd ed., vol. 3. Ohio: Materials Information Soc; 1990. p. 2566–7.
[69] Deledda S, Hauback BC, Fjellvag H. H-sorption behavior of mechanically activated Mg–Zn powders. J Alloys Compd 2007;446–447:173–7.
[70] Sahlberg M, Andersson Y. Hydrogen absorption in Mg–Y–Zn ternary compounds. J Alloys Compd 2007;446–447:134–7.
[71] Andreasen A. Hydrogenation properties of Mg–Al alloys. Int J Hydrogen Energy 2008;33:7489–97.
[72] Wang XL, Tu JP, Zhang PL, Zhang XB, Chen CP, Zhao XB. Hydrogenation properties of ball-milled MgH_2–10 wt% $Mg_{17}Al_{12}$ composite. Int J Hydrogen Energy 2007;32:3406–10.
[73] Crivello JC, Nobuki T, Kato S, Abe M, Kujid T. Hydrogen absorption properties of the γ-$Mg_{17}Al_{12}$ phase and its Al-richer domain. J Alloys Compd 2007;446–447:157–61.
[74] Hiromasa YB, Kuji T. Thermal stability and hydrogen absorption/desorption properties of $Mg_{17}Al_{12}$ produced by bulk mechanical alloying. J Alloys Compd 2007;433:241–5.
[75] Johansson M, Ostenfeld CW, Chorkendorff I. Adsorption of hydrogen on clean and modified magnesium films. Phys Rev B 2006;74:193408.
[76] Zaluska A, Zaluski L, Strom-Olsen JO. Synergy of hydrogen sorption in ball-milled hydrides of Mg and Mg_2Ni. J Alloys Compd 1999;289:197–206.
[77] Spassov T, Rangelova V, Neykov N. Nanocrystallization and hydrogen storage in rapidly solidified Mg–Ni–RE alloys. J Alloys Compd 2002;334:219–23.
[78] Spassov T, Koster U. Nanocrystalline Mg–Ni-based hydrogen storage alloys produced by nanocrystallization. Mater Sci Forum 1999;307:197–202.
[79] Huang LJ, Liang GY, Sun ZB. Hydrogen-storage properties of amorphous Mg–Ni = Nd alloys. J Alloys Compd 2006;421:279–82.
[80] Wu Y, Solberg JK, Yartys VA. The effect of solidification rate on microstructural evolution of a melt-spun Mg–20Ni–8Mm hydrogen storage alloy. J Alloys Compd 2007;446–447:178–82.
[81] Wu Y, Lototskyy MV, Solberg JK, Yartys VA. Effect of microstructure on the phase composition and hydrogen absorption-desorption behaviour of melt-spun Mg–20Ni–8Mm alloys. Int J Hydrogen Energy 2012;37:1495–508.
[82] Wu Y, Lototsky MV, Solberg JK, Yartys VA, Han W, Zhou SX. Microstructure and novel hydrogen storage properties of melt-spun Mg–Ni–Mm alloys. J Alloys Compd 2009;477:262–6.
[83] Wu Y, Han W, Zhou SX, Lototsky MV, Solberg JK, Yartys VA. Microstructure and hydrogenation behavior of ball-milled and melt-spun Mg–10Ni–2Mm alloys. Int J Hydrogen Energy 2008;466:176–81.
[84] Orimo S, Fujii H. Materials science of Mg–Ni-based new hydrides. Appl Phys A 2001;72:167–86.
[85] Wu Y, Lototsky MV, Solberg JK, Yartys VA. Microstructural evolution and improved hydrogenation–dehydrogenation kinetics of nanostructured melt-spun Mg–Ni–Mm alloys. J Alloys Compd 2011;509S:S640–5.
[86] Adelhelm P, de Jongh PE. The impact of carbon materials on the hydrogen storage properties of light metal hydrides. J Mater Chem 2011;21:2417–27.
[87] Nielsen TK, Manickam K, Hirscher M, Besenbacher F, Jensen TR. Confinement of MgH_2 nanoclusters within nanoporous aerogel scaffold materials. ACS Nano 2009;3:3521–8.
[88] Karger ZZ, Hu J, Roth A, Wang D, Kübel C, Lohstroh W, et al. Altered thermodynamic and kinetic properties of MgH_2 infiltrated in microporous scaffold. Chem Coun 2010;46:8353–5.
[89] Paskevicius M, Tian HY, Sheppard DA, Webb CJ, Pitt MP, Gray EM, et al. Magnesium hydride formation within carbon Aerogel. J Phys Chem C 2011;115:1757–66.
[90] Gross AF, Ahn CC, Atta VSL, Liu P, Vajo JJ. Fabrication and hydrogen sorption behaviour of nanoparticulate MgH_2 incorporated in a porous carbon host. Nanotechnology 2009;20:204005.
[91] Tan ZP, Chiu C, Heilweil EJ, Bendersky LA. Thermodynamics, kinetics and microstructural evolution during hydrogenation of iron-doped magnesium thin films. Int J Hydrogen Energy 2011;36:9702–13.
[92] Xin GB, Yang JZ, Wang CY, Zheng J, Li XG. Promising hydrogen storage properties and potential applications of Mg–Al–Pd trilayer films under mild conditions. Dalt Trans 2012;41:6783–90.

[93] Ouyang LZ, Wang H, Chung CY, Ahn JH, Zhu M. MgNi/Pd multilayer hydrogen storage thin films prepared by dc magnetron sputtering. J Alloys Compd 2006;422:58–61.
[94] Zahiri B, Harrower CT, Amirkhiz BS, Mitlin D. Rapid and reversible hydrogen sorption in Mg–Fe–Ti thin films. Appl Phys Lett 2009;95:103114.
[95] Zahiri R, Zahiri B, Kubis A, Kalisvaart P, Amirkhiz BS, Mitlin D. Microstructural evolution during low temperature sorption cycling of Mg-AlTi multilayer nanocomposites. Int J Hydrogen Energy 2012;37:4215–26.
[96] Liu T, Cao YR, Xin GB, Li XG. Superior hydrogen storage and electrochemical properties of Mg_xNi_{100-x}/Pd films at room temperature. Dalt Trans 2013;42:13692–7.